JACS
JOURNAL OF THE AMERICAN CHEMICAL SOCIETY
Communication
pubs.acs.org/JACS

Catalytic Iridium-Based Janus Micromotors Powered by Ultralow Levels of Chemical Fuels

Wei Gao, Allen Pei, Renfeng Dong, and Joseph Wang*

Department of Nanoengineering, University of California, San Diego, La Jolla, California 92093, United States

Supporting Information

ABSTRACT: We describe catalytic micromotors powered by remarkably low concentrations of chemical fuel, down to the 0.0000001% level. These Janus micromotors rely on an iridium hemispheric layer for the catalytic decomposition of hydrazine in connection to SiO_2 spherical particles. The micromotors are self-propelled at a very high speed (of ~20 body lengths s^{-1}) in a 0.001% hydrazine solution due to osmotic effects. Such a low fuel concentration represents a 10 000-fold decrease in the level required for common catalytic nanomotors. The attractive propulsion performance, efficient catalytic energy-harvesting, environmentally triggered swarming behavior, and magnetic control of the new Janus micromotors hold considerable promise for diverse practical applications.

Achieving autonomous motion of nano/microscale objects in the low Reynolds number regime is an exciting yet challenging research area.[1−10] Particular attention has been given over the past decade to chemically powered micromotors that exhibit self-propulsion in the presence of hydrogen peroxide fuel. These primarily include bimetallic catalytic nanowires,[11−13] microtubular microengines,[14−17] and Janus microparticles.[18−21] These chemically powered micromotors commonly require high concentrations of the chemical fuel. Despite extensive efforts to lower the required fuel level, such catalytic micromotors still rely on at least 0.2% (~60 mM) hydrogen peroxide for their operation.[16,22] The requirement of high fuel concentrations greatly hinders the practical utility of catalytically powered nanomotors. In addition, the repertoire of chemical reactions that can impact momentum remains limited primarily to hydrogen peroxide.

Here we introduce a catalytic Janus micromotor that displays efficient propulsion in the presence of extremely low levels of chemical fuel, 10^{-7} to 10^{-3}%, i.e., over a 10 000-fold decrease compared to common catalytic motors. Such low-fuel micromotors have been realized using iridium (Ir)-based Janus microparticles (with an Ir layer on an oxide support surface) in the presence of hydrazine as the sole fuel (Figure 1A). At the macroscale, hydrazine (N_2H_4) is a well-known monopropellant, commonly used in rocket motors.[23] On the other end of the spectrum, a bimetallic catalytic microfluidic pumping system, based on very high hydrazine fuel levels (2%), has been reported.[24] We have previously shown that a hydrazine additive within a high hydrogen peroxide fuel level results in dramatically

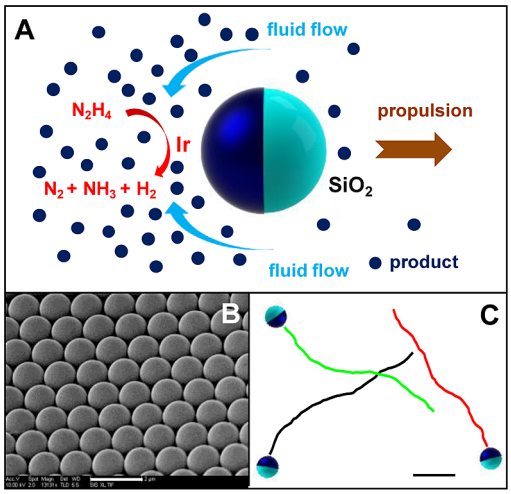

Figure 1. (A) Schematic of catalytic Ir/SiO_2 Janus micromotors powered by hydrazine. N_2, H_2, and NH_3 molecules are generated at the Ir surface, creating a zone of high product concentrations. Fluid flows from the SiO_2 side to the Ir side because of the product gradient. As a result, the motor moves toward the SiO_2 side. (B) Scanning electron microscope (SEM) image of an array of assembled spherical Ir/SiO_2 micromotors. Scale bar, 2 μm. (C) Tracking lines (taken from Supporting Information Video S1) illustrating the distances traveled by three micromotors in a 0.001% hydrazine solution over 1 s. Scale bar, 5 μm.

increased speed for both catalytic nanowire motors and tubular microengines.[13,25]

In the following sections, we will demonstrate that efficient autonomous propulsion of Janus micromotors can be achieved even at trace (ppb) levels of hydrazine alone. The influence of fuel concentrations on the motor speed is investigated and compared to common peroxide-based catalytic Janus micromotors, which display autonomous propulsion due to the oxygen product gradient.[18−21] The propulsion mechanism of the new Ir-based motors is discussed, and its dependence on the composition of the particle support is evaluated. Collective swarming and the resulting micropumping behaviors at low fuel concentrations are also demonstrated.

The Janus micromotors consist of plain silica particles (1.2 μm diameter) with one hemisphere coated with iridium metal. Iridium metal catalyst beds are commonly utilized to decompose hydrazine fuel in monopropellant rockets.[26,27] The Ir surface

Received: December 20, 2013
Published: January 29, 2014

   dx.doi.org/10.1021/ja413002e | J. Am. Chem. Soc. 2014, 136, 2276−2279

catalyzes the decomposition of hydrazine to form nitrogen gas (N_2), hydrogen gas (H_2), and ammonia (NH_3) as products (Figure 1A) in accordance to reactions 1 and 2:[26,27]

$$3N_2H_4 \rightarrow N_2 + 4NH_3 \quad (1)$$

$$3N_2H_4 \rightarrow 2N_2 + 3H_2 + 2NH_3 \quad (2)$$

As a result, a high local concentration of products is formed around the Ir surface, leading to an osmotic gradient and a fluid slip velocity. The diffusiophoretic mechanism causes water to flow from regions of low to high solute concentrations. The induced fluid flow is thus directed around the motor, from the SiO_2 side to the Ir side, propelling the Janus micromotor toward the SiO_2 side. The micromotors are easily fabricated by a directional Ir sputter deposition onto a monolayer of silica microparticles (Figure 1B). As illustrated from the track-lines of Figure 1C and corresponding Supporting Information Video S1, the resulting Ir-SiO_2 Janus motors move rapidly at an average speed of 21 μm/s in a 0.001% hydrazine solution.

In general, diffusiophoretic movement of a particle is caused by a gradient of uncharged (nonelectrolyte) solutes, such as N_2, H_2, and NH_3 in the present system, across the particle surface. This interaction is determined by the absorption strength (Gibbs' absorption length, K), and the length of the solute−surface interaction, L. The velocity of the particle (U) resulting from the solute gradient is described by[28,29]

$$U = \frac{kT}{\eta} KL\nabla C \quad (3)$$

where k is the Boltzmann constant, T is the solution temperature, η is the fluid viscosity, and ∇C is the solute concentration gradient. However, in the case of hydrazine, the products contain not only neutral (N_2, H_2, NH_3) molecules but also a cationic (NH_4^+) species, resulting from the protonation of NH_3 in water. As a result, there are two possible diffusiophoretic mechanisms for the directional propulsion, chemophoretic and osmophoretic, corresponding to electrolyte and nonelectrolyte products, respectively. These mechanisms are opposing, with chemophoretic movement toward higher concentrations and osmophoretic movement directed to lower concentrations.[30] For the present Ir Janus motors, the directional locomotion toward the SiO_2 side confirms the dominating role of the osmotic effects. As the motors continue to move, more hydrazine is reacted and additional cations are produced, resulting in a stronger chemophoretic influence, responsible for the gradual decrease in motor speed over time.

The propulsion of the new Ir-SiO_2 micromotors involves a similar mechanism as that of Pt-based Janus motors, which utilize the O_2 gradient resulting from Pt-catalyzed decomposition of hydrogen peroxide. The track lines of Figure 2A illustrate the motion of common Pt-SiO_2 micromotors in the presence of a high concentration of hydrogen peroxide fuel (10%) with an average speed of 12 μm/s. Using 1% hydrogen peroxide, these Pt-SiO_2 micromotors display no apparent displacement (inset of Figure 2A), analogous to the behavior of common Au−Pt bimetallic nanowire motors.[11−13] In contrast, and as indicated from Figure 2B, the new Ir-SiO_2 Janus motors move with greatly increased speeds of over 20 μm/s in just 0.001% hydrazine fuel. The 10 000-fold excess of fuel required to propel the Pt-Janus motors vs Ir-based Janus motors (Figure 2A vs 2B) highlights the significant advantage of using remarkably low levels of the hydrazine fuel. It should be pointed out that while Pt-SiO_2 Janus motors also displayed directional propulsion at low hydrazine

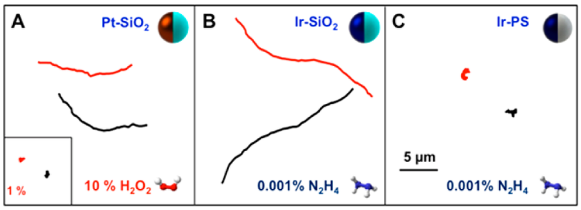

Figure 2. Tracking lines (taken from Supporting Information Video S2) illustrating a typical motion and moving distances of Pt/SiO_2 Janus micromotors (a) in the presence of 10 and 1% (inset) hydrogen peroxide fuel, and of Ir/SiO_2 (b) and Ir/PS (c) micromotors in the presence of 0.001% hydrazine fuel over a 1 s period.

concentrations, other metal catalytic layers (e.g., Pd, Ag) resulted in a greatly diminished movement.

Interestingly, Ir-coated polystyrene (PS) Janus microparticles hardly move under the same conditions, and instead display extremely low movement speeds and short lifetimes (Figure 2C). It is well established that high surface-area oxide surfaces enhance the reactivity of Ir catalysts toward the hydrazine decomposition reaction.[24] Iridium-based Janus micromotors made with PS particles coated with a layer of alumina or titania show improved movement behavior (with a directional speed of 12 μm/s) compared to plain Ir-PS motors (Supporting Information Video S3). Such strong dependence of the movement upon the surface conditions suggests the critical role of the oxide surface supporting the Ir catalytic layer.

The Ir Janus motors are able to retain directional propulsion over a wide range of fuel concentrations and during long periods of more than 10 min. Figure 3 (and corresponding Supporting

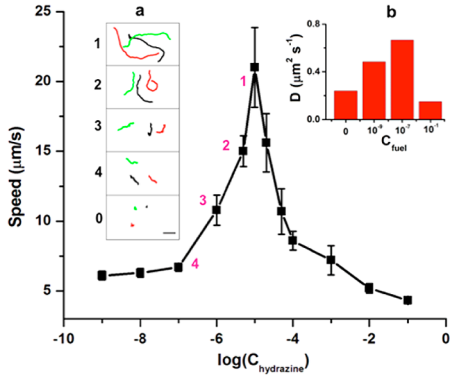

Figure 3. Dependence of the speed of Ir/SiO_2 Janus micromotors upon the hydrazine concentration over the 0.0000001−10% range ($n \geq 50$). Inset (a), tracking lines (taken from Supporting Information Video S4) illustrating the travel distances of the Janus micromotors over a 1 s period in the presence of 0.001% (1), 0.0005% (2), 0.0001% (3), 0.00001% (4) hydrazine, as well as without hydrazine (0). Scale bar, 5 μm. Inset (b), histogram of the diffusion coefficients of the Ir-based Janus micromotors, compared to Brownian motion, in the presence of extremely low levels of hydrazine.

Information Video S4) shows the influence of fuel concentration on the micromotor speed. The motors exhibit a high average speed of 21 μm/s in 0.001% fuel. As expected, the speed decreases upon lowering the fuel level; yet, it remains higher than Brownian motion even at concentrations as low as 0.0000001%. Inset (a) of Figure 3 displays the actual tracked paths of the motors, demonstrating their significant net displacement at extremely low fuel concentrations compared to randomly moving Brownian particles (1−4 vs 0). Enhanced diffusion and

dx.doi.org/10.1021/ja413002e | J. Am. Chem. Soc. 2014, 136, 2276−2279

increased directional mobility are observed even at ppb fuel levels. To clearly indicate the directional movement of the Janus motors at extremely low fuel concentrations, we experimentally estimated the enhanced diffusion coefficients of the motors. The motors ($n \geq 40$) were tracked over 10 s, and the mean squared displacement was calculated at different fuel levels and plotted against time using MATLAB to obtain the diffusion coefficient from the slope. The mean squared displacement, ΔL^2, of the Janus motors has contributions from both directional propulsion and Brownian diffusion. The rotational diffusion coefficient, τ_R, of a particle with radius R can be found from the Stokes–Einstein relation:

$$\tau_R^{-1} = \frac{kT}{8\pi\eta R^3} \tag{4}$$

The mean squared displacement can be approximated by two characteristic equations for time scales far from τ_R:[18]

$$\Delta L^2 = \begin{cases} 4D\Delta t + V^2\Delta t^2, \ \Delta t \ll \tau_R \\ (4D + V^2\tau_R)\Delta t, \ \Delta t \gg \tau_R \end{cases} \tag{5}$$

where D is the diffusion coefficient for a plain particle, Δt is the time, and V is the velocity. For $\Delta t \ll \tau_R$, the propulsion of the particle dominates and ΔL^2 increases quadratically with time, while when $\Delta t \gg \tau_R$, the rotational diffusion of the particle randomizes the 2-dimensional directional movement of the particle, resulting in a random walk with ΔL^2 increasing linearly with time. For these Janus motors with a diameter of 1.2 μm, τ_R is found to be 1.38 s, and the plot of the mean squared distance over 10 s is easily linearly fitted. Inset (b) of Figure 3 shows the increase in diffusion coefficient from 0.24 to 0.48 and to 0.67 $\mu m^2/s$ upon increasing the hydrazine level from 0 to 0.0000001 to 0.00001%, respectively, illustrating the high mobility of the motors (relative to Brownian motion) even in extremely low fuel levels. It should be pointed out that these ppb–ppm hydrazine fuel levels have been shown to exert negligible toxicity on different animals.[31,32] Similar to other chemical fuels, the level of hydrazine may change during practical applications due to reactions with coexisting species.

As illustrated in Figure 3, the speed of Janus micromotors decreases upon increasing the fuel concentrations above 0.001%. This is contrary to the common behavior of catalytic micromotors and is likely due to the inhibiting effects of the ionic species associated with the hydrazine decomposition reaction, namely, partial protonation of the NH_3 to form NH_4^+ (pK_a = 9.25). Solutions containing high hydrazine concentrations also have high pH values (11.58, 10.64, and 10.13 for 10, 1, and 0.1% hydrazine, respectively) because of the formation of $N_2H_5^+$ and OH^- ions:

$$N_2H_4 + H_2O \rightarrow [N_2H_5]^+ + OH^- \tag{6}$$

As a result, the speed and diffusion coefficient of the motors in 10% (0.15 $\mu m^2/s$) hydrazine is even lower than the diffusion coefficient observed without the fuel (0.24 $\mu m^2/s$), i.e., for Brownian motion. Additional experiments indicated reduced speed with increasing salt concentrations. Such ionic-strength effect is consistent with the behavior of H_2O_2-powered Pt-based micromotors.[33] Note that no apparent bubble generation was observed throughout these experiments.

Magnetic control of the directionality of the new Janus micromotor can be achieved through the deposition of a paramagnetic Ni layer. Coating the entire particle with a TiO_2 layer (through atomic layer deposition, ALD) after the Ni deposition results in a uniform oxide support, which can facilitate the Ir-based catalytic reaction. Figure 4A illustrates the layered

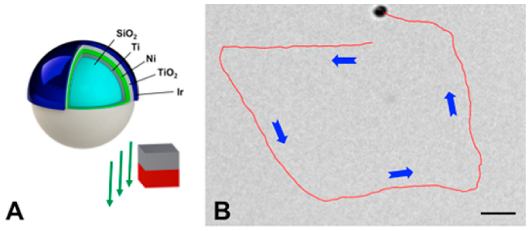

Figure 4. (A) Schematic of the magnetic control of multilayer Ir-TiO_2-Ni-Ti-SiO_2 Janus micromotors. (B) Time-lapse images (taken from Supporting Information Video S5) showing the magnetically guided propulsion of an Ir-TiO_2-Ni-Ti-SiO_2 micromotor in the presence of 0.001% hydrazine. Scale bar, 5 μm.

coatings on the microparticle used for achieving magnetic guidance of the Janus micromotors. These Janus motors can be precisely navigated using an external magnetic field to follow predetermined trajectories (Figure 4B and Supporting Information Video S5). Such magnetic guidance thus offers high spatial and temporal resolution essential for a variety of practical applications. The resulting motors display a high speed of over 30 μm/s, which is higher than that of Ir-SiO_2 micromotors, and can be attributed to the increased surface area of the ALD-fabricated TiO_2 layer.

We also observed that the new hydrazine-driven Janus micromotors display a collective swarming behavior in response to their environment (Figure 5). While a limited aggregation of

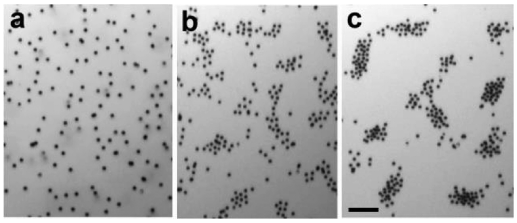

Figure 5. The swarming behavior of the Ir-based micromotors (diameter: 4.74 μm). (a–c) Microscopic images (taken from Supporting Information Video S6) illustrating the time-dependent schooling of the Janus micromotors in presence of 0.001% hydrazine fuel at 0, 2, 4 min, respectively. Scale bar, 50 μm.

the 1.2 μm micromotors was observed in the 0.001% hydrazine solution, increasing the motor size to 4.74 μm resulted in a rapid formation of densely ordered swarms. The gradient-induced swarming of gold microparticles in the presence of high levels of H_2O_2 coupled with N_2H_4 has been reported previously.[34] The new Janus motors autonomously swarm with the sole presence of extremely low levels of hydrazine fuel. The time-lapse images in Figure 5 (corresponding to Supporting Information Video S6) illustrate the spatially organized schooling of the Janus motors at 0, 2, and 4 min after the addition of 0.001% hydrazine (a, b, and c, respectively). This behavior is attributed to the diffusioosmotic and diffusiophoretic effects resulting from the accumulation of nonelectrolyte reaction products. The larger schools of Ir motors remained aggregated for up to 1 h and then began to disperse because of the diminished fuel level and product gradient. However, new school formation can be triggered by readding the hydrazine fuel, indicating a reversible swarming behavior.

dx.doi.org/10.1021/ja413002e | J. Am. Chem. Soc. 2014, 136, 2276–2279

Because of the product concentration gradient and limited propulsion speed of 4.74 μm motors, an inward fluid flux is generated, facilitating the formation of motor swarms. As a result, the smaller schools can continuously attract and draw in neighboring motors, resulting in larger and more tightly packed schools (c). The fluid flows generated around these motor swarms has been visualized (in Supporting Information Video S7) using smaller passive tracer microparticles (1.2 μm in diameter), illustrating the capability of using these motor swarms as efficient micropumps.[35] These micropumps retain their pumping ability over the entire schooling period, indicating considerable promise for nanoscale delivery applications.[36]

In conclusion, we have demonstrated that catalytic micromotors can be powered by extremely low concentrations of chemical fuels. Such hydrazine-propelled iridium-based micromotors display efficient propulsion of over 20 μm/s and require substantially (10 000-fold) lower fuel levels compared to commonly used peroxide-based Pt-based micromotors. This study also represents the first example of the use of hydrazine as the sole fuel for catalytic micromotors. As these Janus micromotors can operate in such low fuel levels, additional studies to further understand their propulsion behavior and efficiency could be extremely useful for designing more efficient micro/nanomachines.[37] Further studies are desired for elucidating the fundamental principles of the propulsion mechanism of such hydrazine-driven Janus micromotors involving both electrolyte and nonelectrolyte products. Future efforts will also aim at exploiting the defined dependence on the hydrazine concentration for sensing applications and for following concentration gradients via chemotaxis. The attractive propulsion and near fuel-free requirements of the new catalytic Janus micromotors hold considerable promise for the design of practical chemically powered nanomachines toward a wide range of important future applications ranging from targeted drug delivery[38] and bioisolation[39] to environmental remediation.[40]

■ ASSOCIATED CONTENT

Supporting Information

Janus micromotors preparation protocols, instrumentation, reagents, and videos. This material is available free of charge via the Internet at http://pubs.acs.org.

■ AUTHOR INFORMATION

Corresponding Author

josephwang@ucsd.edu

Notes

The authors declare no competing financial interest.

■ ACKNOWLEDGMENTS

This project received support from the Defense Threat Reduction Agency-Joint Science and Technology Office for Chemical and Biological Defense (Grant No. HDTRA1-13-1-0002). W.G. is a HHMI International Student Research fellow. The authors also thank R. Tam and I. Rozen for their help.

■ REFERENCES

(1) Wang, J. *Nanomachines: Fundamentals and Applications*; Wiley-VCH: Weinheim, 2013.
(2) Mallouk, T. E.; Sen, A. *Sci. Am.* **2009**, *5*, 72.
(3) Mirkovic, T.; Zacharia, N. S.; Scholes, G. D.; Ozin, G. A. *ACS Nano* **2010**, *4*, 1782.
(4) Wang, J.; Gao, W. *ACS Nano* **2012**, *6*, 5745.
(5) Sanchez, S.; Pumera, M. *Chem.—Asian J.* **2009**, *4*, 1402.
(6) Ozin, G. A.; Manners, I.; Fournier-Bidoz, S.; Arsenault, A. *Adv. Mater.* **2005**, *17*, 3011.
(7) Wang, W.; Duan, W.; Ahmed, S.; Mallouk, T. E.; Sen, A. *Nano Today* **2013**, *8*, 531.
(8) Wilson, D. A.; Nolte, R. J. M.; van Hest, J. C. M. *Nat. Chem.* **2012**, *4*, 268.
(9) Loget, G.; Kuhn, A. *J. Am. Chem. Soc.* **2010**, *132*, 15918.
(10) Loget, G.; Kuhn, A. *Nat. Commun.* **2011**, *2*, 535.
(11) Paxton, W. F.; Kistler, K. C.; Olmeda, C. C.; Sen, A.; St. Angelo, S. K.; Cao, Y.; Mallouk, T. E.; Lammert, P. E.; Crespi, V. H. *J. Am. Chem. Soc.* **2004**, *126*, 13424.
(12) Fournier-Bidoz, S.; Arsenault, A. C.; Manners, I.; Ozin, G. A. *Chem. Commun.* **2004**, 441.
(13) Laocharoensuk, R.; Burdick, J.; Wang, J. *ACS Nano* **2008**, *2*, 1069.
(14) Mei, Y. F.; Huang, G. S.; Solovev, A. A.; Urena, E. B.; Monch, I.; Ding, F.; Reindl, T.; Fu, R. K. Y.; Chu, P. K.; Schmidt, O. G. *Adv. Mater.* **2008**, *20*, 4085.
(15) Mei, Y. F.; Solovev, A. A.; Sanchez, S.; Schmidt, O. G. *Chem. Soc. Rev.* **2011**, *40*, 2109.
(16) Gao, W.; Sattayasamitsathit, S.; Orozco, J.; Wang, J. *J. Am. Chem. Soc.* **2011**, *133*, 11862.
(17) Zhao, G.; Pumera, M. *RSC Adv.* **2013**, *3*, 3963.
(18) Howse, J. R.; Jones, R. A.; Ryan, A. J.; Gough, T.; Vafabakhsh, R.; Golestanian, R. *Phys. Rev. Lett.* **2007**, *99*, 048102.
(19) Gibbs, J. G.; Zhao, Y.-P. *Appl. Phys. Lett.* **2009**, *94*, 163104.
(20) Baraban, L.; Makarov, D.; Streubel, R.; Monch, I.; Grimm, D.; Sanchez, S.; Schmidt, O. G. *ACS Nano* **2012**, *6*, 3383.
(21) Gao, W.; Pei, A.; Feng, X.; Hennessy, C.; Wang, J. *J. Am. Chem. Soc.* **2013**, *135*, 998.
(22) Sanchez, S.; Ananth, A. N.; Fomin, V. M.; Viehrig, M.; Schmidt, O. G. *J. Am. Chem. Soc.* **2011**, *133*, 14860.
(23) Schmidt, E. W. *Hydrazine and Its Derivatives*; Wiley-Interscience: New York, 2001.
(24) Ibele, M. E.; Wang, Y.; Kline, T. R.; Mallouk, T. E.; Sen, A. *J. Am. Chem. Soc.* **2007**, *129*, 7762.
(25) Gao, W.; Sattayasamitsathit, S.; Uygun, A.; Pei, A.; Ponedal, A.; Wang, J. *Nanoscale* **2012**, *4*, 2447.
(26) Contour, J. P.; Pannetier, G. *J. Catal.* **1972**, *24*, 434.
(27) Escard, J. *J. Catal.* **1973**, *29*, 31.
(28) Keh, H. J.; Luo, S. C. *Phys. Fluids* **1995**, *7*, 2122.
(29) Pavlick, R. A.; Sengupta, S.; McFadden, T.; Zhang, H.; Sen, A. *Angew. Chem., Int. Ed.* **2011**, *50*, 9374.
(30) Anderson, J. L. *Annu. Rev. Fluid Mech.* **1989**, *21*, 61.
(31) Re-evaluation of some organic chemicals, hydrazine and hydrogen peroxide. In *IARC Monographs on the Evaluation of the Carcinogenic Risks to Humans*; IARC: Lyon, 1999; Vol. *71*, p 991.
(32) Choudhary, G.; Hansen, H. *Chemosphere* **1998**, *37*, 801.
(33) Ebbens, S.; Gregory, D. A.; Dunderdale, G.; Howse, J. R.; Ibrahim, Y.; Liverpool, T. B.; Golestanian, R. 2013, arXiv:1312.6250.
(34) Kagan, D.; Balasubramanian, S.; Wang, J. *Angew. Chem., Int. Ed.* **2011**, *50*, 503.
(35) Patra, D.; Zhang, H.; Sengupta, S.; Sen, A. *ACS Nano* **2013**, *7*, 7674.
(36) Zhang, H.; Yeung, K.; Robbins, J. S.; Pavlick, R. A.; Wu, M.; Liu, R.; Sen, A.; Phillips, S. T. *Angew. Chem., Int. Ed.* **2012**, *51*, 2400.
(37) Wang, W.; Chiang, T.; Velegol, D.; Mallouk, T. E. *J. Am. Chem. Soc.* **2013**, *135*, 10557.
(38) Gao, W.; Kagan, D.; Pak, O. S.; Clawson, C.; Campuzano, S.; Chuluun-Erdene, E.; Shipton, E.; Fullerton, E. E.; Zhang, L.; Lauga, E.; Wang, J. *Small* **2012**, *8*, 460.
(39) Campuzano, S.; Orozco, J.; Kagan, D.; Guix, M.; Gao, W.; Sattayasamitsathit, S.; Claussen, J. C.; Merkoci, A.; Wang, J. *Nano Lett.* **2012**, *12*, 396.
(40) Guix, M.; Orozco, J.; Garcia, M.; Gao, W.; Sattayasamitsathit, S.; Merkoci, A.; Escarpa, A.; Wang, J. *ACS Nano* **2012**, *6*, 4445.